Journal of Hydroscience and Hydraulic Engineering
Vol. 16, No. 1, May, 1998, 87-96

CHARACTERISTICS OF MEANDERING COMPOUND CHANNEL FLOW EVALUATED WITH TWO-LAYERED, 2-D METHOD

By

H.S. Jin, S. Egashira

Faculty of Science and Engineering, Ritsumeikan University,
1-1-1 Noji-higashi, Kusatsu, Shiga 525, Japan

and

B.Y. Liu

The NEWJEC Consultants, Inc., 20-19 Shimanouchi 1-Chome,
Chuo-ku, Osaka 542, Japan

SYNOPSIS

Based on a numerically-generated boundary-fitted orthogonal curvilinear coordinate system, a 2-layered, 2-D mathematical model for unsteady flows with complicated boundaries is presented. It is employed to evaluate the change of flow patterns such as water surface level, velocity vector, Lagrangian pathline and friction factor in sine-generated meandering compound channel in terms of water depth ratio between in main channel and in flood plain. It is concluded that the over-bank flow is impacted severely by the meandering main channel flow when the flow depth on flood plain is shallow, and is almost independent of that when h_u/h_l (ratio of water depths above and below the floodplain) is greater than 0.9, except the super-elevation of water surface due to the meandering in-bank flow. The bulk friction factor (f or $f/(8C_f)$) changes with h_u/h_l very interestingly.

INTRODUCTION

Most river flows can be characterized as meandering compound channel flows, i.e., consisting of a meandering main channel flanked by one or two side flood plains. Such a flow is absolutely three-dimensional because of the interactions between main flow and flood plain one with large difference in water depth, hydraulic roughness and curvature of channel, etc. The study of compound channel flows is meaningful from both the theoretical and the practical view-points. Many researchers have studied such flows in both experiments and numerical simulations (Ashida *et al.* (2), Ashida *et al.* (3), Liu (7), Murota *et al.* (8), Myers & Brennan (9), Naot *et al.*(10)). Myers and Brennan (9) found from their experiment that the resistance coefficients of main channel and flood plain are increased or decreased, respectively by the presence of the momentum transfer mechanism. Ashida *et al.* (2) demonstrated that a large amount of suspended sediment is dispersed laterally onto the plain and then deposit to the bed due to the reduction of transport capacity. Liu (7) elucidated the basic characteristics of sediment transport with conditions of compound channel flows and the associated phenomena of flow structure and bed deformation. According to energy conservation law, Ashida *et al.* (3) proposed a method to assess the flow resistance in compound channels. On the basis of algebraic stress models and solving the 3-D form of the equations, Naot *et al.* (10)

showed the importance of secondary currents in calculating the transverse momentum transfer in straight compound channel flow.

Although a reliable 3-D hydrodynamic model may be available (10), it is still difficult for most engineering works. One of the difficulties is intensive and expensive computational effort. Nevertheless, it is feasible to develop a two-layered, two-dimensional model which could be taken as a quasi-3D model and might represent compound channel flow well. Such a model can exactly describe the sudden change of water depth between main channel and flood plain and the boundary conditions at the side walls of main channel, and effectively investigate the interactions between layer-averaged main channel flow and overflow, etc. Flow features can be considered vertically homogeneous in each layer and be described in layer-averaged two-dimensional forms approximately, just as depth-averaged model which has been proved to be effective for shallow water flow over whole depth (Abbott (1)), except on the interaction between two layers.

In the paper, a rigorous quasi-3D—two-layered, two-dimensional—mathematical model employing finite difference method is developed for flow with complicated and irregular boundaries, e.g., meandering compound channel flow, etc. For this purpose, the present model utilizes a numerically-generated boundary-fitted orthogonal coordinate which represents complicated boundaries accurately. The method pays attention to the mass and the momentum exchange across the interface between the two layers due to convection and diffusion, though the effect of secondary flow due to curvature of streamlines and so on may be important. Curvature affects the flow in several ways, e.g., super-elevation, secondary current, redistribution of longitudinal velocities, etc. The depth-averaged method may be used to simplify such 3-D curved channel problem into 2-D when the depth-radius ratio is small. In spite of the great efforts made in developments of depth-averaged meandering channel flow models, e.g., some empirical methods based on results of fully developed bend flows are used for considering velocity deviation terms in transverse momentum exchange due to secondary current in the depth-averaged governing equations, their results are still not in perfect on the velocity redistribution and the water surface configuration (Jin & Steffler (5), Kalkwijk & Vriend (6)).

The present model is calibrated and verified first by comparing the computational results of water surface level, velocities and Lagrangian pathline with the measured data in a sine-generated meandering compound flume. Then some numerical tests are conducted by the present method to evaluate the characteristics of meandering compound channel flows in terms of water depth ratio between in the main channel and in the flood plain.

DESCRIPTION OF THE MODEL

Governing Equations for Two-layered-averaged Flow

The hydrodynamic equations solved in the model, apart from the interaction between the layers, are similar to, and are derived in a similar way to, the depth-averaged equations (Abbott (1)), with consideration of mass and momentum exchange between the layers. In shallow areas in which vertical position of the interface between the upper (surface) layer and the lower (bottom) is equal to or lower than that of the bed, the bottom layer vanishes and the surface layer is used only.

For all variables in this paper, subscript "u" and "l" designate the quantity in the upper layer and the lower one respectively; subscript "0", "s" and "b" denote the quantity at the interface between the upper layer and the lower, at free surface and at bed respectively; k=indices of layer: k='u' designates the surface layer and k='l' the bottom one respectively. The definition of layer-averaged variables and derivation of governing equations in detail can be found in Chau and Jin (4).

Layer-averaged continuity and momentum equations in each layer are written as follows:

$$Ct_k + \frac{1}{g_{11}g_{22}}\left[\frac{\partial(g_{22}h_k u_k^*)}{\partial\xi} + \frac{\partial(g_{11}h_k v_k^*)}{\partial\eta}\right] = 0 \qquad (1)$$

$$\frac{\partial(h_k u_k^*)}{\partial t}+\frac{1}{g_{11}g_{22}}[\frac{\partial(g_{22}h_k u_k^{*2})}{\partial \xi}+\frac{\partial(g_{11}h_k u_k^* v_k^*)}{\partial \eta}+h_k v_k^*(u_k^*\frac{\partial g_{11}}{\partial \eta}-v_k^*\frac{\partial g_{22}}{\partial \xi})]=$$
$$-\frac{h_k g}{g_{11}}\frac{\partial \zeta}{\partial \xi}+\frac{1}{g_{11}g_{22}}[\frac{\partial(h_k g_{22}\sigma_{1k})}{\partial \xi}+\frac{\partial(h_k g_{11}\tau_{21k})}{\partial \eta}+h_k(\tau_{12k}\frac{\partial g_{11}}{\partial \eta}-\sigma_{2k}\frac{\partial g_{22}}{\partial \xi})]+M_{\xi k} \quad (2)$$

$$\frac{\partial(h_k v_k^*)}{\partial t}+\frac{1}{g_{11}g_{22}}[\frac{\partial(g_{22}h_k u_k^* v_k^*)}{\partial \xi}+\frac{\partial(g_{11}h_k v_k^{*2})}{\partial \eta}+h_k u_k^*(v_k^*\frac{\partial g_{22}}{\partial \xi}-u_k^*\frac{\partial g_{11}}{\partial \eta})]=$$
$$-\frac{h_k g}{g_{22}}\frac{\partial \zeta}{\partial \eta}+\frac{1}{g_{11}g_{22}}[\frac{\partial(h_k g_{22}\tau_{12k})}{\partial \xi}+\frac{\partial(h_k g_{11}\sigma_{2k})}{\partial \eta}+h_k(\tau_{21k}\frac{\partial g_{22}}{\partial \xi}-\sigma_{1k}\frac{\partial g_{11}}{\partial \eta})]+M_{\eta k} \quad (3)$$

where $Ct_u=\partial\zeta/\partial t-w_0$, $Ct_l=-\partial Z_b/\partial t+w_0$, $M_{\xi u}=w_0u_0^*+(\tau_{s\xi}-\tau_{0\xi})/\rho$, $M_{\eta u}=w_0v_0^*+(\tau_{s\eta}-\tau_{0\eta})/\rho$, $M_{\xi l}=-w_0u_0^*+(\tau_{0\xi}-\tau_{b\xi})/\rho$, $M_{\eta l}=-w_0v_0^*+(\tau_{0\eta}-\tau_{b\eta})/\rho$; u_k^*, v_k^* = ξ and η components of layer-averaged velocity in k-th layer, respectively; ζ, Z_b = water surface level and bed elevation, respectively; $h_u(=\zeta-Z_0)$, $h_l(=Z_0-Z_b)$ = water depth in the surface layer and the bottom, respectively; Z_0 = vertical position of the interface and Z_0=const unless $Z_0=Z_b\neq$const in the shallow areas; u_0^*, v_0^*, w_0 = ξ, η and z (positive vertically upward) components of velocity at the interface, respectively; ρ, g = density of water and acceleration due to gravity (=9.8m/s^2), respectively. $\tau_{s\xi}$, $\tau_{s\eta}$, $\tau_{0\xi}$, $\tau_{0\eta}$ and $\tau_{b\xi}$, $\tau_{b\eta}$ = ξ, η components of shear stress on the water surface, on the interface and on the bed respectively which may also include the contribution of horizontal stresses due to the spatial variation of free surface and bed elevation. σ_{1k}, σ_{2k}, τ_{12k}, τ_{21k} = layer-averaged effective stresses resulted from turbulence, etc. in k-th layer and are described according to the Boussinesq's approximation for turbulent stresses (Rodi (11)), please see Chau & Jin (4) for the detail descriptions. g_{11}, g_{22}, J = orthogonal coordinate transformation relationships (Chau & Jin (4), Thompson *et al.* (12)).

The bed shear stress is expressed empirically as depth-averaged method except its direction according to velocity components in the bottom layer

$$\frac{\tau_{b\xi}}{\rho}=u_*^2\frac{u_l^*}{\sqrt{u_l^{*2}+v_l^{*2}}} \quad ; \quad \frac{\tau_{b\eta}}{\rho}=u_*^2\frac{v_l^*}{\sqrt{u_l^{*2}+v_l^{*2}}} \quad (4)$$

where $u_*(=[C_f(u^{*2}+v^{*2})]^{1/2})$ = friction velocity, herein $u^*=(h_uu_u^*+h_lu_l^*)/h$, $v^*=(h_uv_u^*+h_lv_l^*)/h$ and $h=\zeta-Z_b$. C_f= resistance coefficient at bed and is determined by the following formula in accordance with the assumption of logarithmic law of velocity distribution: $C_f=1/[6.0+\kappa^{-1}\ln(h/k_s)]^2$, $\kappa(\approx0.4)$ = von Karman constant (11) and k_s = roughness height at bed. The surface shear stress is ignored here.

The shear stress at the interface between two layers is represented approximately as follows (see Chau & Jin (4) for its detail description):

$$\frac{\tau_{0\xi}}{\rho}=\varepsilon_{m0}\frac{\partial u^*}{\partial z}\approx\varepsilon_{m0}\frac{u_u^*-u_l^*}{\delta} \quad ; \quad \frac{\tau_{0\eta}}{\rho}\approx\varepsilon_{m0}\frac{v_u^*-v_l^*}{\delta} \quad ;$$
$$\varepsilon_{m0}=\kappa h_l(1-\frac{h_l}{h})u_* \quad ; \quad l_0=\kappa h_l(1-\frac{h_l}{h})^{1/2} \quad (5)$$

where ε_{m0}= turbulent viscosity on the vertical direction at the interface, l_0= Prandtl mixing length and δ= mixing layer thickness at the interface. Herein, $\delta=l_0$.

In the model, no equation may be used to calculate the horizontal velocity components(u_0^*, v_0^*) at the interface. Herein, $u_0^* \approx (h_u u_l^* + h_l u_u^*)/h$ and $v_0^* \approx (h_u v_l^* + h_l v_u^*)/h$ (4). The vertical velocity (w_0) at the interface, which results in convective exchange between two layers, can be calculated from layer-averaged continuity equation after obtaining the solutions of horizontal velocities and water surface level.

Boundary and Initial Conditions

An impenetrable condition is specified at the side wall and the tangential velocity is not zero. When discretizing the momentum equations at the grids near side wall, the shear stress on the wall is substituted with an empirical formula similar to eq. 4. After linearizing relevant terms in the momentum equations, the solution of velocities can be obtained without directly knowing the specific tangential velocity on the boundary. The water surface elevation (ζ) at the side wall can be determined by the normal component of momentum equation.

Velocity at the upstream boundary and water surface level at the downstream end are specified in the present model. In the following calculations, the water surface level at the downstream exit is specified according to the measured data in the verification case and that of nearly uniform flow condition in the cases of numerical test. The corresponding discharge which is converted into velocity with Chezy's empirical formula is employed at the upstream boundary.

Besides boundary conditions, initial conditions are also indispensable for closing the above unsteady governing equations. In the model, the initial conditions are obtained by interpolating the corresponding boundary conditions at starting time (t=0).

Numerical Scheme

The computational domain is shown in Fig. 1(a). An unified numerically-generated boundary-fitted orthogonal coordinate system is used in both the surface and the bottom layers. The computational grids which are "staggered" for velocities and water surface level are displayed in Fig. 1(a), (b) and (c).

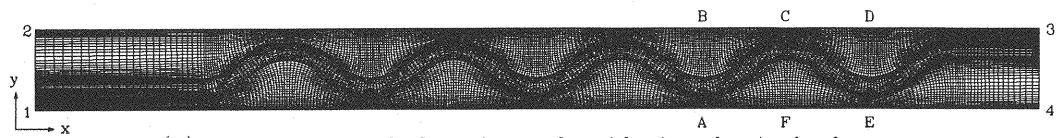

(a) Computational domain and grids in physical plane

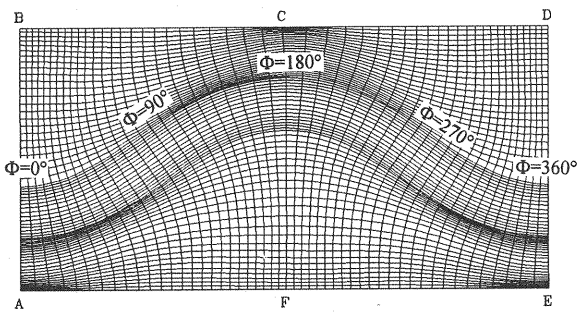

(b) Local grids

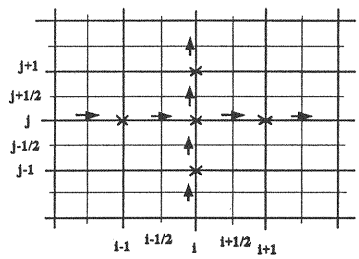

(c) Schematic grids in transformed plane and 'staggered' grid system (× ζ; →u_0^*, u_l^*; ↑v_0^*, v_l^*)

Fig. 1 Computational domain and grid system

A special finite difference method is presented to achieve the numerical solution of the above governing equations.

In order to calculate water surface level, the depth-averaged continuity equation which is obtained by combining the above layer-averaged continuity equations is solved first. Therein, nonlinear terms are linearized as, $h_u u_u^* = (\zeta - Z_0)u_u^* = \zeta^{n+1}u_u^{*n} + (\zeta^n - Z_0)\tilde{u}_u^* - \zeta^n u_u^{*n}$, $h_l u_l^* = (Z_0 - Z_b)\tilde{u}_l^*$ and the corresponding approximations are made for $h_u v_u^*$ and $h_l v_l^*$. Herein "~" means temporary variables which have their relevant relationships with ζ at time $(n+1)\Delta t$ according to the corresponding momentum equations, e.g., $\tilde{u}^*_{k\ i+\frac{1}{2},j} = A^u_{k,e}(\zeta^{n+1}_{i+1,j} - \zeta^{n+1}_{i,j}) + B^u_{k,e}$, $\tilde{v}^*_{k\ i,j+\frac{1}{2}} = A^v_{k,n}(\zeta^{n+1}_{i,j+1} - \zeta^{n+1}_{i,j}) + B^v_{k,n}$. $A^u_{k,e}$, ..., $B^v_{k,n}$ and so forth are the coefficients which could be calculated. Δt is the time step and the index 'n' denotes the time level of the discretized hydrodynamic variables. i and j are the node numbers in the ξ and η direction, respectively. Thus, a linearized algebraic equation set about water surface level could be expressed as

$$a_{Pi,j}\zeta^{n+1}_{i,j} = a_{Ei,j}\zeta^{n+1}_{i+1,j} + a_{Wi,j}\zeta^{n+1}_{i-1,j} + a_{Ni,j}\zeta^{n+1}_{i,j+1} + a_{Si,j}\zeta^{n+1}_{i,j-1} + b_{i,j} \qquad (6)$$

where $a_{Pi,j}$, $a_{Ei,j}$, $a_{Wi,j}$, $a_{Ni,j}$, $a_{Si,j}$ and $b_{i,j}$ = coefficients. Solving the above equation set by Tri-Diagonal Matrix Algorithm (TDMA) with Alternating Direction Iteration (ADI), the water surface elevation ζ^{n+1} at time $(n+1)\Delta t$ can be obtained.

Then, the momentum equations are discretized under new water surface level ζ^{n+1} with backward finite difference for the time derivation, first-order upwind finite difference for the advection terms and the diffusion terms by spatial central finite difference scheme. A linearization method, i.e., some variables in the nonlinear terms are partially replaced with their corresponding values at the beginning of this time step (time=$n\Delta t$), is exerted during discretization. These result in an implicit numerical algorithm. The algebraic equation sets are solved iteratively by TDMA and we can get the solution of velocities.

COMPARISON OF THE COMPUTATIONAL RESULTS WITH MEASURED DATA

The present model is calibrated and verified with experimental flume data (Liu (7)). The flume is 12m long and 1m wide with a central located main channel. The main channel is 20cm wide and 3cm deep, and its centerline is taken as sine-generated-curve in which the maximum angular deviation of the centerline θ_{max} from x-axis is 35° and the wave length L along the centerline is 2.2m. Four and a half waves are formed, as shown in Fig. 1(a) and (b). The flume slope is 0.009. The mean diameter of bed material is 1.3mm and the bed is inerodible. Fig. 2 shows the representative cross-sections of the meandering compound channel. The interface between two layers in the model is located at Z_0=3cm which is the location of floodplain. h_u and h_l in Fig. 2 are the water depths above and below the interface, respectively.

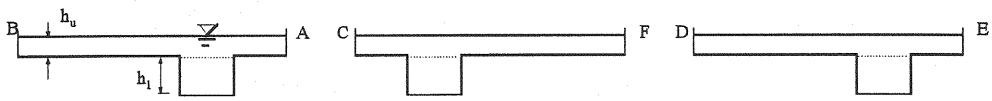

(a) B-A section (b) C-F section (c) D-E section

Fig. 2 Schematic cross-sections

The computed results of the case for discharge of 7.15 l/s and mean water depth of about 4.4cm in main channel are compared with the measurements. The computed water surface level and measured data are displayed in Fig. 3. It shows that the predicted result mimics well the measured one in both magnitude and shape of water surface. The method could reproduce well the super-elevation due to the effect of streamline curvature. With attention focused on the flow along main channel, the transversal gradients of water surface near the bend top (Φ = 0°, 180° and 360°) are more uniform than those in other locations. Near Φ = 90° and 270°, the transversal gradients in the inner bank are steep and those in the outer bank are gentle. The longitudinal gradients in the flood plains are gentle in the regions with Φ of 30°~180° on the left side and Φ of 210°~360° on the right side, and inversely those are steep in the regions with Φ of 0°~150° on

the left and Φ of 180°~330° on the right side, which are consistent with the variations of free surface in the main channel. Such water surface patterns would be resulted from the back water effect induced by the swell-head in the concave and the lower in the convex of the meandering main channel flow surface due to curvature of streamline.

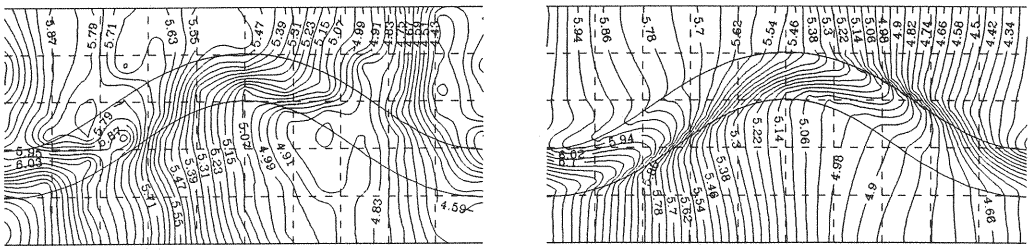

(a) Measured (b) Predicted

Fig. 3 Water surface level contour (unit: cm)

Fig. 4 shows the flow fields in both layers. The computed velocity vectors agree with the measured data though difference exists somewhere. The phenomena of velocity redistribution occurred. In the main channel, over-bank velocity direction is obviously different from that in the in-bank. The region of maximum in-bank velocity shifts gradually from the outer bank-convex to the inner-bank-convex and the velocity at the convex bank reaches a maximum just before the bend top, and the minimum one inversely. The over-bank flow tends to meander due to the effects of meandering main channel flow and its variation takes place in a similar way as found in the in-bank. Affected by the meandering main channel, flow on the flood plains tends to main channel in its direction and an according pattern of velocity redistribution occurred.

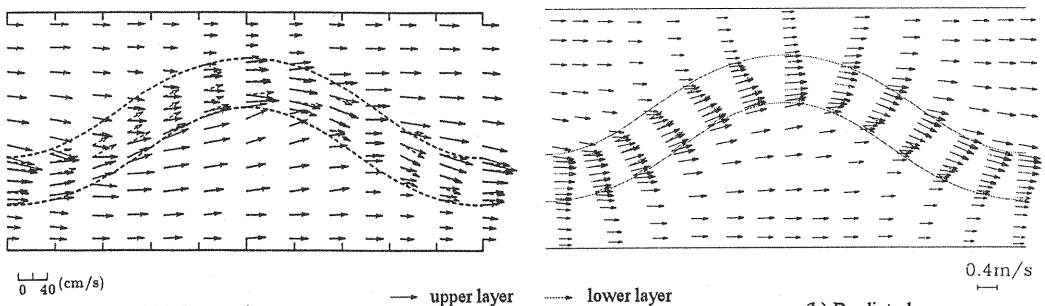

(a) Measured (b) Predicted

Fig. 4 Two-layered flow fields in the meandering compound channel

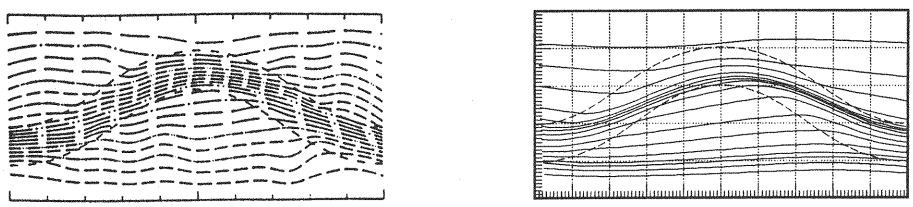

(a) Measured depth-averaged streamline (b) Computed over-bank Lagrangian Pathline

Fig. 5 Measured depth-averaged streamline and computed over-bank Lagrangian pathline

The measured depth-averaged streamlines and the computed over-bank-averaged Lagrangian pathlines in which the starting points are located at the grid points of section A-B in Fig. 1(b) are shown in

Fig. 5. Due to the meandering main channel, the flow on flood plains tends to the main channel and the over-bank flow in the main channel follows the flow in the in-bank. Such a flow pattern can be evaluated very well by the method.

These and the results of aforementioned super-elevation and velocity redistribution show that the method represents the two-layered, two-dimensional sine-generated meandering compound channel flow very well.

CHARACTERISTICS OF MEANDERING COMPOUND CHANNEL FLOW IN TERMS OF h_u/h_l

The meandering compound channel flow is affected by many factors. Among these factors, water depth ratio, width one and roughness one between in main channel and in flood plains, geometry of meandering main channel and flood plains and so on might be most important. Herein, the above method is employed to evaluate the effect of water depth ratio (h_u/h_l=0.11~5.06) between in main channel and in flood plains on meandering compound channel flow under the constant main channel Froude number (=0.72) and the same geometry as above. The flume slope is reset according to the conditions of constant main channel Froude number and nearly uniform flow. The boundary conditions for the calculations are specified accordingly.

The computed free surface contours are listed in Fig. 6. When the flow on flood plains is very shallow, e.g., h_u/h_l=0.24, the longitudinal gradient of free surface in flood plains and the transversal one in main channel do not vary sharply. With increase of h_u/h_l, the free surface tends to become severely uneven, as stated in former section. When it exceeds 0.9, relatively flat and steep areas of longitudinal gradient are formed on the flood plains. The former expands to the main channel and the latter contracts with increase of h_u/h_l. At the flow depth ratio of 3, a very sharp transversal variation of water surfaces forms near the inner bank region with Φ of about 45°~135° and near the outer bank region with Φ of about 225°~315°, as shown in Fig. 6.

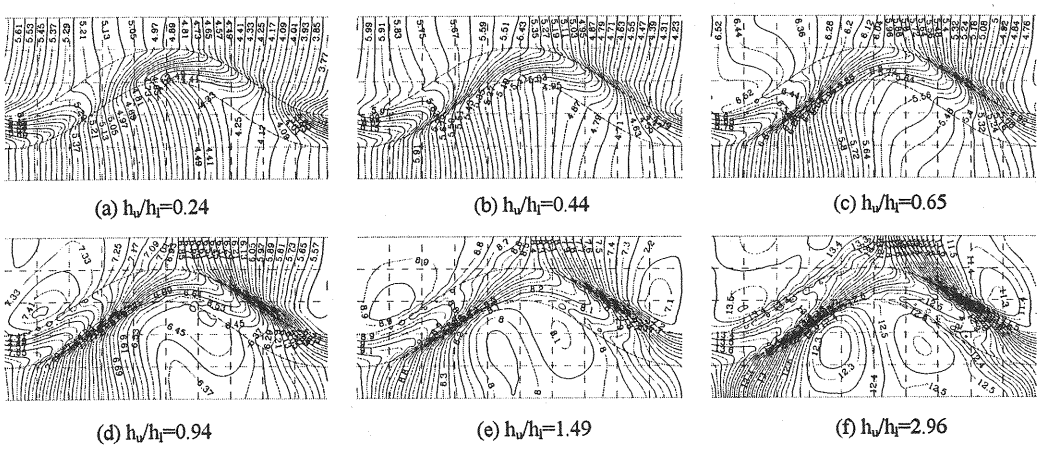

(a) h_u/h_l=0.24 (b) h_u/h_l=0.44 (c) h_u/h_l=0.65

(d) h_u/h_l=0.94 (e) h_u/h_l=1.49 (f) h_u/h_l=2.96

Fig.6 Computed free surface configurations of the meandering compound channel flow with h_u/h_l (unit: cm)

The computed over-bank Lagrangian pathlines are shown in Fig. 7. They become straight with increase of h_u/h_l, i.e., the over-bank flow tends to be independent of the meandering main channel.

Fig. 8 shows the results of bulk friction factor ($f = 8gRi_e/V^2$, R is the hydraulic radius, V is the section-averaged velocity, i_e is the longitudinal slope of water surface) with h_u/h_l. C_f in Fig. 8(b) refers to one in the main channel. f is affected by the bed, side wall, transverse momentum exchange and so on, and herein C_f is only determined by the relative bed roughness, h/k_s. Fig. 8(a) demonstrates a very meaningful feature. When the flow on the flood plains is very shallow, the main channel flow is dominant and the friction conforms with the law in single channel. With increase of h_u/h_l, f first increases rapidly with h_u/h_l because the

transverse momentum exchange plays a key role at this stage and reaches a peak (0.0945) at h_u/h_l=0.35, then decreases to a valley (0.0765) at h_u/h_l=1.2 due to weakening of the influence of momentum exchange. When h_u/h_l exceeds 1.2, f almost increases linearly with h_u/h_l and conforms a similar law as in single channel. At this stage, effect of side wall is more dominant than the momentum exchange. The relationship between $f/(8C_f)$ and h_u/h_l supports the above analysis. When h_u/h_l=0.11, f is almost equivalent to C_f. It means that effect of the bed is a primary factor under such condition. Hereafter, $f/(8C_f)$ raises drasticly with h_u/h_l and reaches a peak value at 0.4 of h_u/h_l due to the reason analysed as above. From 0.4 to 0.95 of h_u/h_l, there is only a slight fall on $f/(8C_f)$ with h_u/h_l. A relatively stable proportion is kept between bed friction and others. $f/(8C_f)$ approximately increases linearly when h_u/h_l is greater than 1 because of strengthening of the effect of side wall.

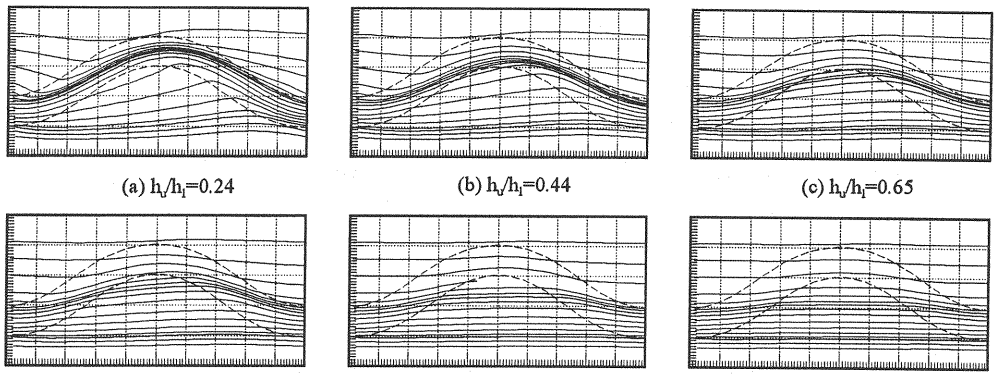

(a) h_u/h_l=0.24 (b) h_u/h_l=0.44 (c) h_u/h_l=0.65

(d) h_u/h_l=0.76 (e) h_u/h_l=1.2 (f) h_u/h_l=2.0

Fig. 7 Over-bank Lagrangian pathline of the meandering compound channel flow

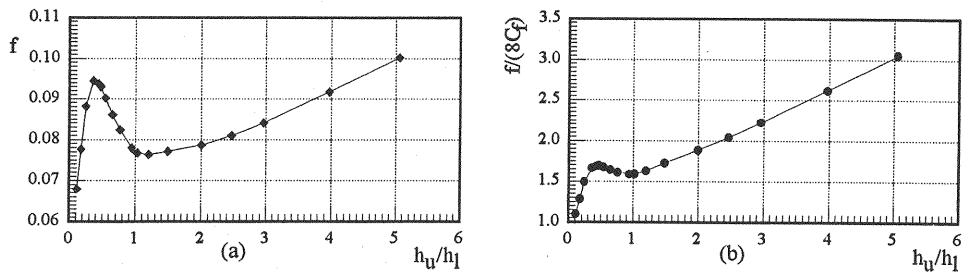

Fig. 8 Bulk friction coefficient versus h_u/h_l (Fr=0.72)

CONCLUSIONS

A quasi-3D, i.e., 2-layered and 2-dimensional, mathematical model with finite difference method based on a numerically-generated boundary-fitted orthogonal coordinates, which can be used to simulate unsteady flows with complicated topography, is developed first. The model is calibrated and verified with experimental results in a sine-generated meandering compound flume. The comparison of the results on water surface, velocity vector and Lagrangian pathline with the experiment data shows that the present model behaves well in reproducing the 2-layered, 2-D meandering compound channel flow.

The method is employed to analyse meandering compound channel flow in terms of relative water depth in main channel and flood plain. It is found from the results of free surface and over-bank Lagrangian pathline that the flow on the flood plains is affected severely by the meandering main channel when h_u/h_l is small. Such influence becomes weak with increase of h_u/h_l. The over-bank flow on the flood plains becomes

almost independent of the main channel when h_u/h_l exceeds 0.9. However the super-elevation of water surface due to meandering in-bank flow exists even if h_u/h_l reaches 3. Due to the different importance of the bed, momentum exchange, side wall and other factors on the flow resistance at different stage of h_u/h_l, there is a very interesting feature on the bulk friction factor with h_u/h_l.

REFERENCES

1. Abbott, M.B. : Computational Hydraulics: elements of the theory of free surface flows, Ashgate Publishing Limited, U.K., 1979.
2. Ashida, K., M. Fujita, B.Y. Liu and T. Tanaka : Transport of suspended sediment in channel with flood plain, Annuals of the Disaster Prevention Research Institute, Kyoto University, No.30(B-2), pp.407-419, 1987 (in Japanese).
3. Ashida, K., S. Egashira and B.Y. Liu : A study of the hydraulics of meandering compound channel flows, Proceedings of Hydraulic Engineering, JSCE, Vol.34, pp.397-402, 1990 (in Japanese).
4. Chau, K.W. and H.S. Jin : Numerical simulation of two-layered, two-dimensional tidal flow in boundary-fitted orthogonal curvilinear coordinate system, International Journal for numerical method in fluids, Vol.21, No.11, pp.1087-1107, 1995.
5. Jin, Y.C. and P.M. Steffler : Predicting flow in curved open channels by depth-averaged method, Journal of Hydraulic Engineering, ASCE, Vol.119, No.1, pp.109-124, 1993.
6. Kalkwijk, J.P. and H.J. de Vriend : Computation of the flow in shallow river bends, Journal of Hydraulic Research, Vol.18, No.4, pp.327-341, 1980.
7. Liu, B.Y. : Study on sediment transport and bed evolution in compound channels, Doctoral Dissertation, Kyoto University, 1991.
8. Murota, A., T. Fukuhara and M. Seta : Hydraulic characteristics of compound channel flows with rough floodplains, Proceedings of Hydraulic Engineering, JSCE, Vol.34, pp.409-414, 1990 (in Japanese).
9. Myers, W.R.C. and E.K. Brennan : Flow resistance in compound channels, Journal of Hydraulic Research, Vol.28, No.2, pp.141-155, 1990.
10. Naot, D., I. Nezu and H. Nakagawa : Hydrodynamic behavior of compound rectangular open channel, Journal of Hydraulic Engineering, ASCE, Vol.119, No.3, pp.390-408, 1993.
11. Rodi, W : Turbulence Models and Their Application in Hydraulics, state-of-the-art, IAHR Publication, DELFT, The Netherlands, 1980.
12. Thompson, Joe F., Z.U.A. Warsi and C.W. Mastin : Numerical Grid Generation—foundations and applications, Elsevier Science Publishing Co., Inc., New York, 1985.

APPENDIX - NOTATION

The following symbols are used in this paper:

$a_{Pi,j}$, $a_{Ei,j}$, ..., $b_{i,j}$ = coefficients;

C_f = resistance coefficient at bed;

f = bulk friction factor ($= 8gRi_e/V^2$);

Fr = Froude number;

g = acceleration due to gravity;

g_{11}, g_{22}, J = orthogonal coordinate transformation coefficients;

h = water depth (ζ-Z_b);

h_l, h_u = water depths in the bottom layer and the surface (ζ-Z_0 and Z_0-Z_b respectively);

i_e = longitudinal slope of water surface;

k_s = roughness height at bed;

l_0 = Prandtl mixing length;

R = hydraulic radius;

u_0^*, v_0^*, w_0 = ξ, η and z (positive vertically upward) components of velocity at the interface, respectively;

u_* = friction velocity;

u^*, v^* = ξ and η components of depth-averaged velocity, respectively;

u_k^*, v_k^* = ξ and η components of layer-averaged velocity in k-th layer, respectively;

V = section-averaged velocity;

Z_0 = vertical position of the interface;

Z_b = bed elevation;

δ = mixing layer thickness at the interface;

ε_{m0} = turbulent viscosity on the vertical direction at the interface;

κ = von Karman constant;

θ_{max} = maximum angular deviation of sine-generated channel from x-axis;

ρ = density of water;

σ_{1k}, σ_{2k}, τ_{12k}, τ_{21k} = layer-averaged effective stresses in k-th layer;

$\tau_{0\xi}$, $\tau_{0\eta}$ = ξ, η components of shear stress on the interface, respectively;

$\tau_{b\xi}$, $\tau_{b\eta}$ = ξ, η components of shear stress on the bed, respectively;

$\tau_{s\xi}$, $\tau_{s\eta}$ = ξ, η components of shear stress on the water surface, respectively;

ξ, η = coordinate components in the orthogonal curvilinear coordinate system;

ζ = water surface level;

Subscripts

0, s, b = quantities at the interface between the upper layer and the lower one, at free surface and at bed, respectively;

i, j = node numbering in ξ and η direction, respectively;

k = indices of layer ('u' for surface layer and 'l' for bottom one respectively);

u, l = quantities in the upper layer and the lower one, respectively; and

Superscript

n = time level of variables.

(Received February 27, 1997; revised January 12, 1998)